

Analysis of subsurface crack propagation under rolling contact loading in railroad wheels using FEM

Yongming Liu, Liming Liu, Sankaran Mahadevan *

Vanderbilt University, Nashville, TN 37235, USA

Received 31 August 2006; received in revised form 2 February 2007; accepted 5 February 2007

Available online 23 February 2007

Abstract

A general subsurface crack propagation analysis methodology for the wheel/rail rolling contact fatigue problem is developed in this paper. A three-dimensional elasto-plastic finite element model is used to calculate stress intensity factors in wheels, in which a sub-modeling technique is used to achieve both computational efficiency and accuracy. Then the fatigue damage in the wheel is calculated using a previously developed mixed-mode fatigue crack propagation model. The advantages of the proposed methodology are that it can accurately represent the contact stress of complex mechanical components and can consider the effect of loading non-proportionality. The effects of wheel diameter, vertical loading amplitude, initial crack size, location and orientation on stress intensity factor range are investigated using the proposed model. The prediction results of the proposed methodology are compared with in-field observations.

© 2007 Elsevier Ltd. All rights reserved.

Keywords: Rolling contact fatigue; Fracture; Crack propagation; Mixed-mode crack; Railroad wheels

1. Introduction

In recent years, higher train speeds and increased axle loads have led to larger wheel/rail contact forces. Also, efforts have been made to optimize wheel and rail design to improve the performance and reduce the cost. These trends have changed the major wheel rim damage from wear to fatigue [1]. Unlike the slow deterioration process of wear, fatigue causes abrupt fractures in wheels or the tread surface material loss. These failures may cause damage to rails, damage to train suspensions and, in some cases, serious derailment of the train.

The fatigue problem of railroad wheels is often referred to as rolling contact fatigue [2], which is caused by repeated contact stress during the rolling motion. Similar fatigue problems also exist in other mechanical components experiencing rolling contact loading, such as gears and bearings. A detailed overview of the rolling contact problem of railroad wheels was given by Ekberg and Kabo [3]. Different failure modes have been

* Corresponding author. Tel.: +1 615 322 3040; fax: +1 615 322 3365.
E-mail address: Sankaran.Mahadevan@vanderbilt.edu (S. Mahadevan).

Nomenclature

p	contact pressure
μ	friction coefficient
τ_{xy}	shear stress
τ_{yz}	shear stress
u_{rel}	relative displacement between the upper crack surface and the lower crack surface
u_{upper}	absolute displacements of the upper crack surfaces
u_{lower}	absolute displacements of the lower crack surfaces
a	crack length
$K_{\text{mixed,eq}}$	equivalent stress intensity factor range under mixed-mode loading
$f\left(\frac{da}{dN}\right)$	crack growth curve obtained under mode I loading
k_1	loading parameters
k_2	loading parameters
k_3	loading parameters
k^H	loading parameters
s	material parameter related to the material ductility
t_{-1}	shear fatigue limit
f_{-1}	tensile fatigue limit
A, B	material parameter
$[\sigma]$	remote stress matrix
$[T]$	transformation matrix from the coordinate system xyz to $x'y'z'$
(ϕ, θ, ψ)	Euler angles
γ	the angle between maximum normal stress amplitude plane and critical plane
delta K	stress intensity factor range
$\frac{da}{dN}$	crack growth rate
ΔK_{eff}	effective stress intensity factor range for mixed-mode loading
R	stress ratio
C	material parameter in Walker's model
m	material parameter in Walker's model
ζ	material parameter in Walker's model
ΔF	applied vertical loading range
$Y(a)$	geometry function considering the effect of crack configuration and boundary conditions
$N(a)$	number of cycle to grow a crack from the initial length a_0 to the length of a_c

observed for railroad wheels, such as shattered rim, vertical split rim and thermal cracking [4]. Shattered rim failures are the result of large subsurface cracks that propagate roughly parallel to the wheel tread surface [5,6]. Thermal cracking usually breaks off a piece of the wheel tread, while shattered rim can destroy the wheel's integrity and thus is more dangerous. The current study focuses on the subsurface crack propagation (shattered rim) analysis.

There are two major groups of models for subsurface fatigue crack analysis under rolling contact loading. One is the group of fatigue crack *initiation* prediction models based on the S–N or ϵ –N curve approach. The other is the group of fatigue crack *propagation* prediction models based on fracture mechanics. These two types of approaches are briefly discussed below.

- (1) *Fatigue crack initiation models*: Bernasconi et al. [7] examined several multiaxial fatigue models by using Hertz contact theory for the wheel material. Guo and Barkey [8] used a 2D finite element model and a multiaxial fatigue model developed by Fatemi and Socie [9] for bearing rolling contact fatigue analysis. Sraml et al. [10] use the Hertz contact theory to calculate the stress response and treat the multiaxial fatigue problem as a uniaxial fatigue problem. The principal stress/strain component in one direction

is used for fatigue analysis. Ringsberg [11] developed a semi-analytical approach for stress calculation, which used 3D finite element analysis but applied the contact pressure based on Hertz theory. The multi-axial fatigue model is a critical plane-based model which uses the damage parameter proposed by Jiang and Sehitoglu [12]. Ekberg et al. [13] developed a fatigue life prediction methodology for the wheel/rail contact fatigue problem, which uses the Hertz contact theory for stress calculation and multi-axial fatigue model proposed by Dang Van et al. [14].

- (2) *Fatigue crack propagation models*: Guagliano and Vergani [15] proposed a semi-analytical approach for the analysis of internal cracks in wheels, in which the finite element method with the applied Hertz contact loading is used to calculate the stress intensity factors. A recent study [16] used a three-dimensional finite element method to calculate the stress intensity factors in hypoid gears. Lansler and Kabo [17] used a 2D finite element model for the analysis of subsurface crack face displacements in railway wheels. Bogdański and Trajer [18] used a plane strain finite element model and the applied Hertz contact pressure for the analysis of stress intensity range in rolling contact fatigue. Glodež and Ren [19] combined a finite element analysis with applied Hertz contact pressure and a mixed-mode crack growth model based on strain energy release rate for the fatigue crack propagation analysis. Cho and Komvopoulos [20] and Komvopoulos [21] used a finite element analysis with applied Hertz contact pressure and a mixed-mode crack propagation model based on the maximum stress intensity factor in mode II.

Most of the existing rolling contact fatigue models use a simplified stress calculation technique, such as Hertz analytical solution or simplified finite element analysis with applied Hertz contact pressure. Due to the complex geometry of the wheel/rail contact area, it is more appropriate to use a 3D finite element method to calculate stress response in the mechanical components. The Hertzian theory assumes that the contact area is small compared to body dimension and surface curvature. It has been shown that the Hertz contact theory is not appropriate when the contact area between wheel and rail is near the wheel flange, where the surface curvature is comparable to the contact area [4]. Liu et al. [4] proposed a finite element computational methodology to calculate the complex 3D stress histories of wheel/rail contact. The stress histories were used for fatigue crack initiation life prediction using the multi-axial fatigue theory developed by Liu and Mahadevan [22].

Most of the existing studies of subsurface crack propagation ignore the non-proportionality of the stress intensity factors. Some of them used a simplified mixed-mode crack propagation model, such as strain energy release rate model [19]. Feng et al. [23] observed different crack growth behavior under proportional and non-proportional loading paths with identical loading magnitude and stated that the models based on the strain energy release rate cannot represent this trend. In Section 2 of this paper, it is shown that the subsurface crack intensity factor histories are non-proportional under rolling contact conditions. A mixed-mode crack propagation model, which can consider the effect of loading non-proportionality, is required for the crack propagation and fatigue life prediction for railroad wheels under this condition.

A general methodology for subsurface fatigue crack propagation analysis of railroad wheels is proposed in this paper. It combines a 3D finite element model for the wheel/rail contact analysis and a mixed-mode crack propagation model previously developed by Liu and Mahadevan [24]. The model predictions are compared with field observations of shattered rim failure of railroad wheels. Parametric studies are performed using the proposed methodology for different vertical loadings, wheel diameters, crack geometries and crack face frictions.

2. Finite element modeling of subsurface crack in wheel/rail contact

Liu et al. [4] proposed a finite element computational methodology for rolling contact analysis of railroad wheels. It has several advantages compared with previous analytical and numerical approaches. First, it is a realistic 3D finite element model and can accurately calculate the 3D stress response in the contact region. Second, it includes both material and geometric non-linearity, i.e. elasto-plastic material behavior and contact stress analysis. It can be used to simulate large and complex wheel motions, such as rotation, sliding, hunting movement and even dynamic impact response. Finally, through sub-modeling techniques, the proposed model is made efficient in computing and hardware requirements. Liu et al. [4] used the model for fatigue crack initiation analysis. In this section, the previous developed finite element model is extended for subsurface crack

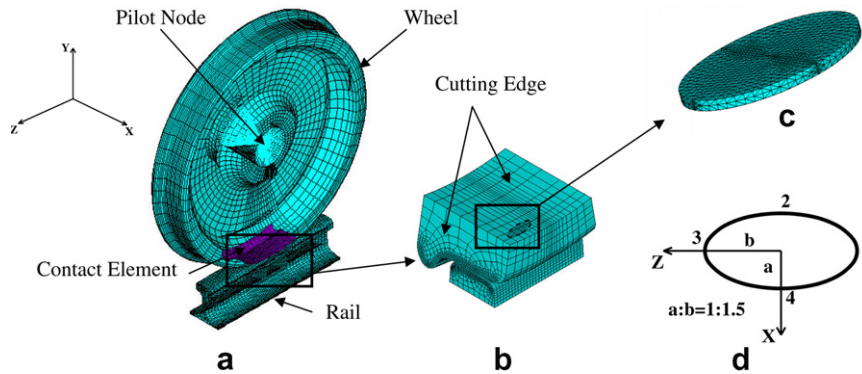


Fig. 1. Finite element modeling of wheel/rail contact with subsurface crack: (a) full model, (b) sub-model, (c) crack and (d) crack shape.

propagation analysis. A brief description of the developed finite element computational methodology is given below, followed by the modification to include a subsurface crack into the wheel.

First, use the available profiles to build the geometry model of the wheel and a piece of rail. This model is called the full model as shown in Fig. 1a. The rail length equals the length between two sleepers. Fixed boundary conditions are applied to the two ends of the rail. Different 3D element sizes are used in the full model (SOLID 45 in ANSYS). Due to the non-linearity of contact analysis, contact surface need fine mesh for accurate stress analysis. In the current study, a finer mesh (the average element length is about 3 mm) is used near the contact region, i.e. near wheel tread surface and rail head surface. At the wheel center, a pilot point is connected to the wheel using rigid link elements. All the external loading and boundary conditions of the wheel are applied on the pilot point. These loading and boundary conditions can be obtained through field measurements or from numerical simulation of the track system motion analysis. The wheel/rail contact surfaces and two crack faces are modeled as surface-to-surface contact elements. The augmented Lagrangian method [25] is used for contact simulation. The friction model is the Coulomb friction model. The Coulomb friction model defines an equivalent shear stress τ , which is proportional to the contact pressure p and the friction coefficient μ . For the wheel/rail contact surface, the friction coefficient (μ) is determined to be 0.3 based on our in-field data from railroad industries, which has been published in our recent study [4]. The material properties of the wheel and rail as described using a linear kinematic hardening model in ANSYS. No isotropic hardening is included in the current model.

Next, quasi-static analysis is performed for the full model and the results for each step are stored. Then the geometry model of the contact region is cut out to create a sub-model as shown in Fig. 1b. The size of the sub-model depends on the analysis objective and also on the wheel motion simulated. The same types of elements as those in the full model analysis are used to mesh the sub-model. A very fine mesh is used in the contact area and to some depth under the contact surface. The results of the full model are interpolated on the cutting edge of the sub-model corresponding to different calculation steps, and the interpolation results are applied as boundary conditions to the sub-model.

An elliptical crack is built into the sub-model, as shown in Fig. 1b. The crack location and orientation are determined from a previous numerical prediction of the initial fatigue crack profile [4], which is consistent with field observations of subsurface crack in railroad wheels. The major axis is along the track direction and the minor axis is perpendicular to the track direction. Based on the field observations of the initial fatigue crack profile, the aspect ratio of the elliptical crack is assumed to be 1.5. The subsurface crack is modeled as two contact surfaces to prevent the surface penetration of the subsurface crack. The Coulomb friction model is used similar to the contact surface between rail and wheel. The friction coefficients between two crack faces are hard to measure and are assumed to vary from 0 to 0.5. Their effects are studied by parametric studies later in this paper. Since our focus is the four crack tips located at the end of major axis and minor axis for the fatigue life prediction, the mesh around the four crack tips are very fine mesh (the average element length is about 0.07 mm) and meshes near other crack front are relatively coarse mesh (the average element length is about 0.5 mm).

In sub-modeling, the results from the sub-model need to be verified to make sure that the cut boundaries are far enough from the stress concentration (contact region and crack tip in this problem). The results in the sub-model are obtained using a fine mesh. They need not agree with the results from coarse mesh full model. The disagreement can be caused not only by mesh refinement differences, but also due to geometric and material non-linearities around the contact region. The cutting edge results from the sub-model analysis are compared with those results in the full model. If the difference is small enough, output the results in sub-model for fatigue crack propagation analysis. Otherwise, change the sub-model and repeat the previous steps.

The finite element models of the full model, sub-model and crack are shown in Fig. 1. The wheel profile is chosen according to the AAR standard [26] wide flange contour. The wheel diameter is 0.914 m (36 in.). From our collected field observations, crack usually occurs at depth 5–10 mm with 20° inclination. The parameter study in our previous paper [4] also shows that cracks initiates at a depth of 5–7 mm and 20° direction. In the current study, the subsurface crack is assumed to be 6 mm below the tread surface with an inclination angle of 20°. The 20° inclination is the angle between the minor axis of the crack and the XZ-plane (Fig. 1). The semi-minor axis is 5 mm. The vertical load applied on the wheel is assumed to be the maximum design load, which is 146.2 kN (32,875 lb). The material properties of the rail and wheel are assumed to be same (yielding strength = 500 MPa; Young's Modulus = 205 GPa; Tangent modulus = 4000 MPa; Friction coefficient = 0.3). The rail length is 600 mm, which is typically the length between two sleepers. In the current study, the initial contact point is assumed to occur at the railhead center and wheel tread center.

The static load analysis of the wheel/rail contact is performed first. The results of the sub-model are shown in Figs. 2 and 3. Fig. 2 shows the von Mises stresses from two different section views. Fig. 3 shows two in-plane

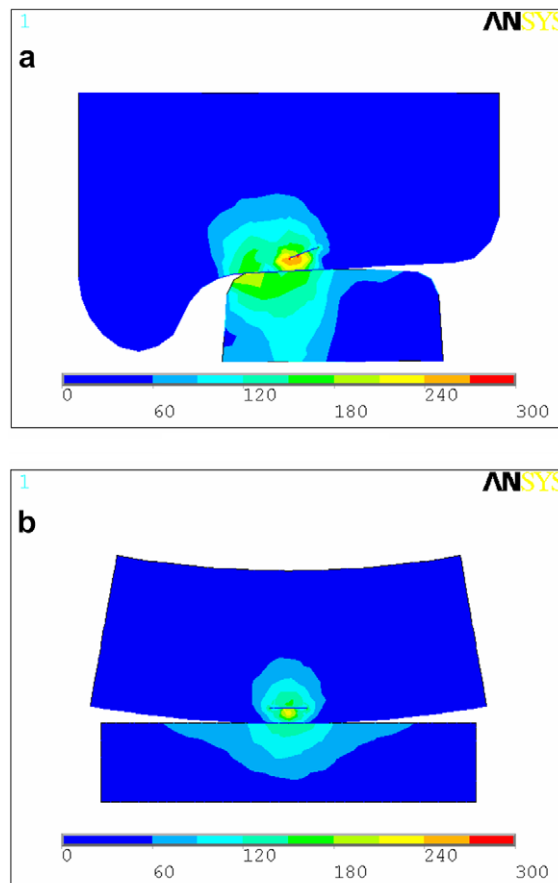


Fig. 2. von Mises stress distribution of wheel/rail contact with subsurface crack (unit: MPa): (a) front section view and (b) left section view.

shear stresses (τ_{xy} and τ_{yz}) from two different section views. From Fig. 2, it is found that the maximum von Mises stress occurs at some depth below the tread surface. The stress decreases quickly as the depth increases. The maximum von Mises stress also occurs around the crack tip, which is caused by the stress concentration near the crack tip. From Fig. 3, a butterfly pattern of the shear stress τ_{yz} is observed. The maximum value occurs at the crack tip. Figs. 2 and 3 show that the high stress only occurs within a small region of the contact location. The stress in the other parts of the model is almost zero. This indicates that only a small portion of the motion simulation is needed because the stress far away from the contact location is negligible.

After performing the static analysis, the wheel rotation on the rail, which is the normal motion mode of the wheel, is simulated. This is done by applying the proper boundary conditions on the pilot node in the full model. For 3D elasto-plastic contact analysis, it is usually very time-consuming, even using the sub-modeling techniques. It is important to use the steady-state stress response within the mechanical components for the fatigue life prediction. We followed the method described in Liu et al. [4] to balance the computational effort and analysis accuracy for the current 3D finite element model. The stress responses after two cycles are assumed to be stabilized values and used for fatigue life prediction.

The current study focuses on subsurface crack behavior under rolling contact loading. The crack deformation behavior is studied first. A relative displacement is defined same as Lansler and Kabo [17]

$$u_{\text{rel}}(\text{I, II, III}) = u_{\text{upper}}(\text{I, II, III}) - u_{\text{lower}}(\text{I, II, III}) \quad (1)$$

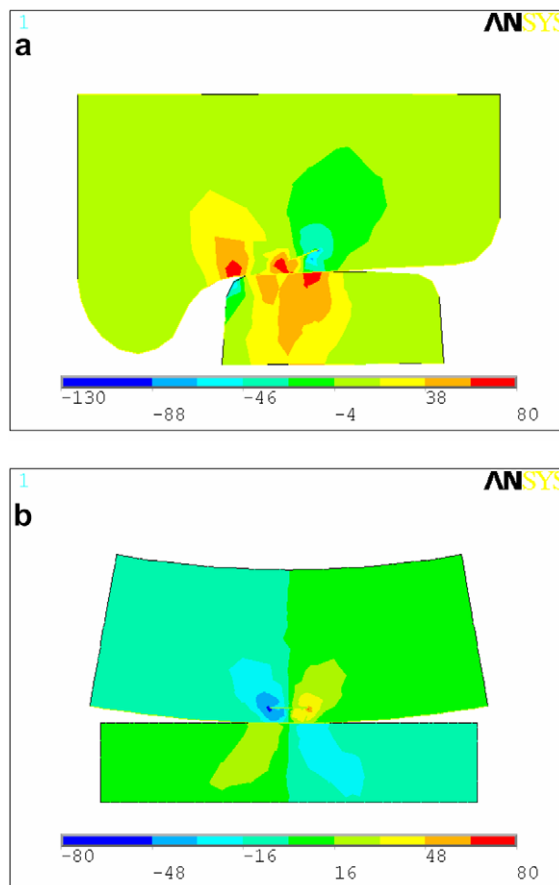


Fig. 3. In-plane shear stress distribution of wheel/rail contact with subsurface crack (unit: MPa): (a) distribution of τ_{xy} and (b) distribution of τ_{yz} .

where u_{rel} is the relative displacement between the upper crack surface and the lower crack surface. u_{upper} and u_{lower} are the absolute displacements of the upper and lower crack surfaces, respectively. (I, II, III) indicates the three modes of crack deformation, i.e. mode I, mode II and mode III, respectively.

The maximum relative displacements along the major and minor axes are shown in Fig. 4. Due to the possible non-proportionality of the stress intensity histories in the three modes, these maximum values may not occur simultaneously. Fig. 4 shows that both mode II and mode III components are significant and must be included in the fatigue crack propagation analysis. During rolling contact, the crack surfaces are closed and the mode I component is not significant, which indicates that the shattered rim failure is driven by shear stress. Compared with the larger mode II and mode III displacements, mode I displacement is small and its effect is ignored in the current study.

The mode II and III stress intensity factor (SIF) histories of crack tips at the major axis and the minor axis (points 1, 2 and 4 in Fig. 1d) during the second revolution of the wheel rotation are shown in Fig. 5. The x -axis does not indicate real time and is the time step in FE analysis during the simulation of wheel rotating. The incremental rotating angles is 0.75° per step. Fig. 5 shows that the SIF in the wheel under rolling contact condition is not proportional, which indicates that the maximum SIFs in mode II and mode III do not occur simultaneously.

The FEA results only show very small residual stresses at these two locations (non-zero SIF values at the beginning and end of the calculation in Fig. 5). We checked the plastic deformation in the FEA analysis and found that the plastic deformation in the current analysis is not very large. The maximum plastic strain along the major crack axis (points 1 and 3) is less than 0.01%. The maximum plastic strain along the minor crack axis (points 2 and 4) is larger but is less than 0.1%. We found that the residual stress is small compared to the applied stress amplitude and its effects are assumed to be negligible in the current study.

3. Mixed-mode fatigue crack propagation model

As shown in Section 2, the subsurface crack in railroad wheels experiences non-proportional mixed-mode loading during rolling contact conditions. Liu and Mahadevan [24] proposed a method for mixed-mode

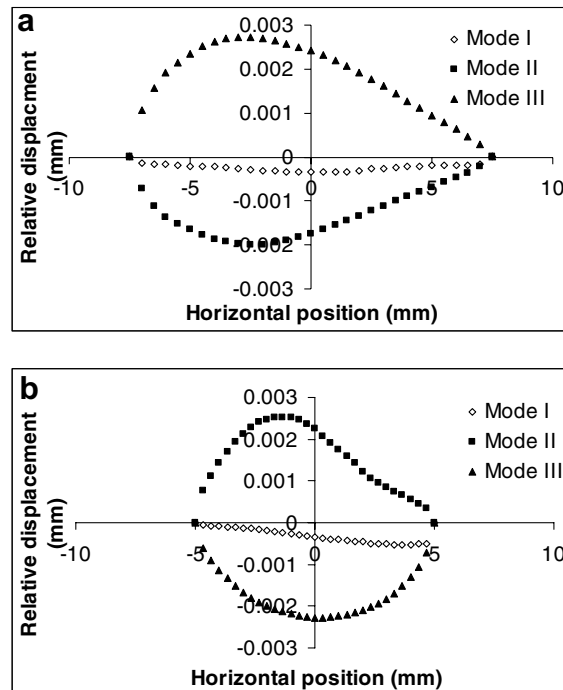


Fig. 4. Relative crack surface displacement: (a) major axis and (b) minor axis.

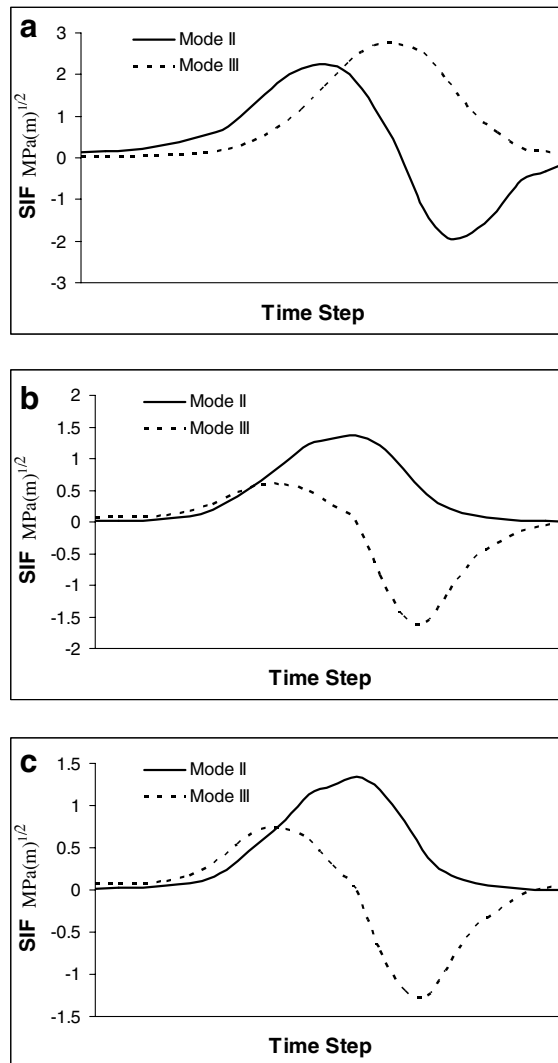


Fig. 5. Stress intensity factor history under rolling contact: (a) point 1, (b) point 2 and (c) point 4.

fatigue crack propagation analysis and the model is used in this paper for rolling contact fatigue analysis of railroad wheels. Only a brief description of the model and the results are shown here. A detailed derivation and explanation of the model can be found in [24].

Liu and Mahadevan [24] examined several available models for mixed-mode fatigue crack propagation and found that most of the available models are only applicable to a limited range of materials (e.g. brittle or ductile metals) and to proportional loadings. The available mixed-mode fatigue crack propagation model is not appropriate for rolling contact fatigue analysis as railroad wheels experience non-proportional cyclic loadings under rolling contact. A previously developed critical plane-based multiaxial fatigue model [22] has been shown to have no limitations with respect to material properties and loading paths. Different from earlier critical plane-based models, the critical plane in [22] is explicitly related to the applied loading and the material's ductility. The plane experiencing maximum normal stress amplitude is first identified. The angle (γ) between the critical plane and the maximum normal stress amplitude plane depends on different materials. For brittle materials, the critical plane is close to the maximum normal stress amplitude plane. For ductile materials, the critical plane is close to the maximum shear stress amplitude plane. Thus this model can automatically adapt for different failure modes, i.e. tensile or shear dominated failure. The model is load path-dependent since different loading paths result in different critical plane orientations and thus different fatigue life prediction.

The developed multiaxial fatigue model can be extended to fracture mechanics-based fatigue crack propagation analysis using the Kitagawa–Takahashi diagram [27]. According to the Kitagawa–Takahashi diagram, the fatigue limit can be expressed using the fatigue crack threshold stress intensity factor and a fictional crack length a . The crack length a represents the intersection of the smooth specimen fatigue limit and the LEFM (linear elastic fracture mechanics) fatigue crack threshold stress intensity factor. One of the important advantages of the Kitagawa–Takahashi diagram is that it links the fatigue behavior of cracked and non-cracked material together, which makes it possible to extend a classical fatigue limit criterion to be a fracture mechanics-based fatigue crack threshold criterion.

Liu and Mahadevan [24] developed a mixed-mode fatigue crack threshold criterion based on the critical plane-based multiaxial fatigue limit criteria [22] and the Kitagawa–Takahashi diagram [27]. After developing the fatigue crack threshold criterion, the methodology for fatigue crack growth rate prediction is relatively easy. The fatigue crack threshold stress intensity factor range is often related to the stress intensity factor range at a very low crack growth rate ($da/dN < 10^{-8}$ – 10^{-7} mm/cycle). For prediction corresponding to an arbitrary crack growth rate da/dN , the fatigue crack threshold stress intensity factors range may be replaced by the stress intensity factor coefficients at the specific crack growth rate. Then the mixed-mode fatigue crack threshold criterion can be used for fatigue crack propagation analysis. The general crack propagation equation is expressed as [24]

$$K_{\text{mixed,eq}} = \frac{1}{B} \sqrt{(k_1)^2 + \left(\frac{k_2}{s}\right)^2 + \left(\frac{k_3}{s}\right)^2 + A \left(\frac{k^H}{s}\right)^2} = f\left(\frac{da}{dN}\right) \tag{2}$$

where $K_{\text{mixed,eq}}$ is the equivalent stress intensity factor range under mixed-mode loading. $f\left(\frac{da}{dN}\right)$ is the crack growth curve obtained under mode I loading. k_1, k_2, k_3 and k^H are the loading parameters with the same unit as the stress intensity factor range. They are defined as remote stress range multiplying $\sqrt{\pi a}$. The details about the calculation of these parameters can be found in [24]. The material parameter $s = \frac{\epsilon-1}{\epsilon-1}$ is related to the material ductility and affects the critical plane orientation. a is the half length of the crack. The subscripts 1, 2, 3 indicate the directions of the stress amplitude as shown in Fig. 6. The superscript H indicates the hydrostatic stress related term. s is the ratio of mode II and mode I stress intensity factors under a specific crack growth rate (da/dN). A and B are material parameters and are listed in Table 1.

Under general three-dimensional non-proportional loadings, a numerical search algorithm is required to identify the critical plane. An efficient procedure similar to our previous method [4] is used in this paper and is described as below.

Consider the stress transformation equation

$$[\sigma]_{x'y'z'} = [T][\sigma]_{xyz}[T]^T \tag{3}$$

where $[\sigma]$ is the remote stress matrix, subscripts xyz and $x'y'z'$ refers to the two coordinate systems (Fig. 6). $[T]$ is the transformation matrix from the coordinate system xyz to $x'y'z'$. $[T]$ consists of nine direction cosines, in

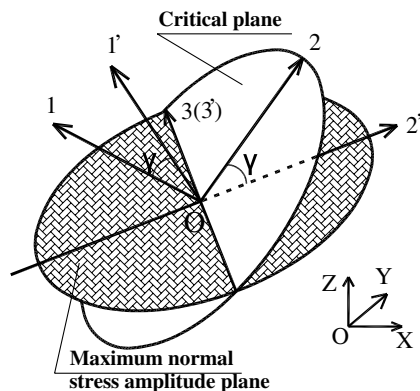


Fig. 6. Schematic illustration of stress components on the critical plane.

Table 1
Material parameters for fatigue crack propagation prediction

Material property	$s = \frac{t-1}{f-1} \leq 1$	$s = \frac{t-1}{f-1} > 1$
γ	$\cos(2\gamma) = \frac{-2 + \sqrt{4 - 4(1/s^2 - 3)(5 - 1/s^2 - 4s^2)}}{2(5 - 1/s^2 - 4s^2)}$	$\gamma = 0$
A	$A = 0$	$A = 9(s^2 - 1)$
B	$B = [\cos^2(2\gamma)s^2 + \sin^2(2\gamma)]^{\frac{1}{2}}$	$B = s$

which only three of them are independent because of the orthogonality conditions. For convenience in numerical calculation, $[T]$ matrix is described using Euler angles (ϕ, θ, ψ) which represent three counterclockwise rotations following the so-called x -convention definition [28]. If the Euler angles are given, the transformation matrix $[T]$ can be written as

$$[T] = \begin{bmatrix} c_\psi c_\phi - c_\theta s_\phi s_\psi & c_\psi s_\phi + c_\theta c_\phi c_\psi & s_\psi s_\theta \\ -s_\psi c_\phi - c_\theta s_\phi c_\psi & -s_\psi s_\phi + c_\theta c_\phi c_\psi & c_\psi s_\theta \\ s_\theta s_\phi & -s_\theta c_\phi & c_\theta \end{bmatrix} \quad (4)$$

where c and s correspond to cosine and sine function, subscripts represent the arguments of such functions. The general ranges for Euler angles (ϕ, θ, ψ) are $[0, 2\pi]$, $[0, \pi]$ and $[0, 2\pi]$, respectively. However, because we only calculate the stress amplitude along one direction, no difference is made if the direction is reversed. The Euler angle ranges can be reduced to $[0, \pi]$ for all three angle parameters (ϕ, θ, ψ) . Furthermore, if we rotate the coordinate system along any original axis by $\pi/2$, the stress matrix components are same except in a different arrangement. During the calculation, we reduce the Euler angle ranges to $[0, \pi/2]$ for all three angle parameters (ϕ, θ, ψ) and search for all three direction stress amplitudes by angle increments of 2° . The normal vector of maximum principal stress amplitude plane is named as $1'$. On the plane perpendicular to $1'$, we search for the maximum shear stress amplitude by rotating the coordinate system about $1'$ axis by angle increments of 2° . The vector of the maximum shear stress amplitude direction on the plane is named as $2'$. $1'$, $2'$ and $3'$ (perpendicular to both $1'$, $2'$) can be treated as a new orthogonal coordinate system (Fig. 6). After obtaining the new $O1'2'3'$ coordinate system, we can calculate the critical plane based on Table 1. Rotate $O1'2'3'$ about $3'$ axis by an angle of γ° to be the new coordinate system $O123$ (Fig. 6). The plane $O23$ is the critical plane. Once the critical plane is identified, Eq. (2) together with the material parameters defined in Table 1 are used for fatigue crack propagation rate prediction under general mixed-mode loading.

As shown in Liu and Mahadevan [22], the ratio of mode II and mode I fatigue crack threshold stress intensity factors s relates to different material failure mechanisms. A larger value of s ($s > 1$) indicates tensile dominated failure and a smaller value of s ($s = \frac{1}{\sqrt{3}}$) indicates shear dominated failure. If the value of s is known, the proposed model can automatically adapt for different failure mechanisms.

The stress intensity factors history obtained from finite element analysis are used to calculate the stress intensity factor range (ΔK) for crack propagation analysis. The mixed-mode crack propagation model is used to calculate the equivalent ΔK in mixed-mode loading and crack propagation profile in railroad wheels. Several different models with different initial crack sizes are analyzed (as shown in the fourth section of parametric study) and the relationship between crack size and ΔK is used for fatigue life prediction. The uniaxial fatigue crack propagation curve is reported by Kuna et al. [29] for a ductile wheel iron. The pure torsional fatigue crack propagation curve is not reported in this study. The value of the ratio s is assumed to be 0.6, which is typical for ductile metals [22,24]. The stress ratio effect is included in the crack propagation using the well-known Walker [30] model. The subsurface crack propagation studied in this paper is shear dominated (mode II and mode III). In our mixed-mode crack growth mode, all modes of SIFs are transformed to be an equivalent SIF and correlate with material's mode I crack growth curve for life prediction. For mode II and mode III SIFs, their stress ratio is either 0 or a finite negative value close to -1 depending on their locations

(see Fig. 4). Thus, the stress ratio of transformed equivalent SIF is also in the range of 0 and a finite negative value. Walker’s model is applicable in this regard. The general crack propagation function is expressed as

$$\frac{da}{dN} = C \left(\frac{\Delta K_{\text{eff}}}{(1 - R)^\zeta} \right)^m \tag{5}$$

where $\frac{da}{dN}$ is the crack growth rate. ΔK_{eff} is the effective stress intensity factor range for mixed-mode loading. For uniaxial fatigue loading, ΔK_{eff} is the mode I stress intensity factor range. R is the stress ratio, and C , m and ζ are material parameters. For the data reported by Kuna et al. [29], C , m and ζ are determined by regression analysis as $5.8e^{-9}$, 2.95 and 1, respectively.

The equivalent mixed-mode delta K can be expressed as a function of applied loading and crack length as

$$\Delta K_{\text{eff}} = \Delta F \sqrt{\pi a} Y(a) \tag{6}$$

where ΔF is the applied vertical loading range. $Y(a)$ is a geometry function considering the effect of crack configuration and boundary conditions, which is calibrated using the finite element results. It should be noted that Eq. (6) is valid if friction is constant or friction effect is small enough to be ignored. In the parametric studies in this paper, we have shown that friction effects are not significant under the current conditions and Eq. (6) can be used. Substituting Eq. (6) into Eq. (5), the fatigue life is expressed as

$$N(a) = \frac{1}{C(\Delta F)^m} \int_{a_0}^{a_c} \frac{(1 - R)^{\zeta m} da}{(\sqrt{\pi a} Y(a))^m} \tag{7}$$

where $N(a)$ is the number of cycle to grow a crack from the initial length a_0 to the length of a_c .

In the current study, the crack shape is assumed to be controlled by four points on the crack front (points 1–4 in Fig. 1d). The crack front profile is approximated using an elliptical curve. The crack growths along the major and minor axes are calculated using the proposed method. The crack front contours at different numbers of cycles are shown in Fig. 7. The increment of number of cycles between each contour is 1.5×10^6 . A couple of field observations of the crack are also shown for comparison. Notice that the current analysis is deterministic and uses the constant maximum design loading for wheels. Thus the current comparison is only

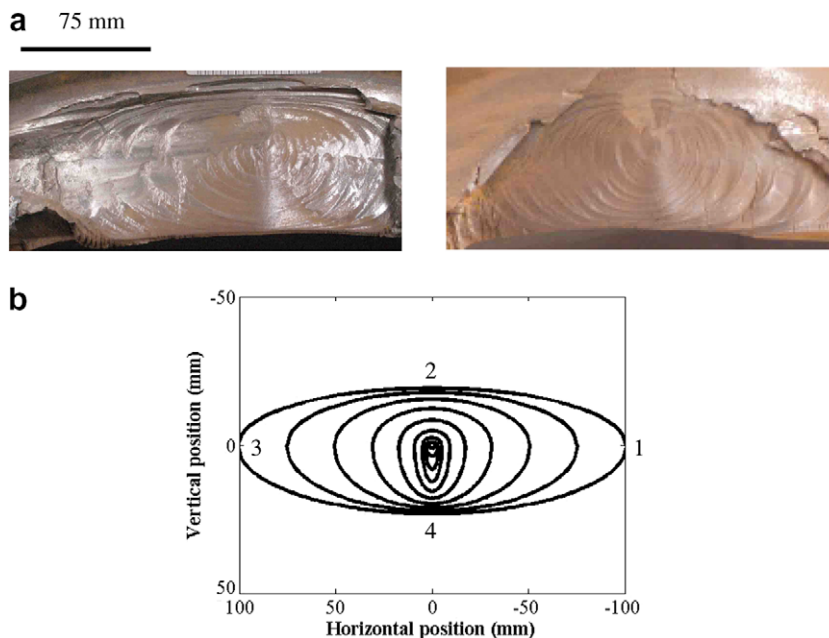


Fig. 7. Crack shape comparison between numerical prediction and field observation: (a) field observations of crack shape and (b) numerical prediction and field observation.

qualitative. A quantitative life prediction comparison between the numerical simulation and field observations must include variability in loading spectra, material properties and structural details. It has been found that the scatter in time to shattered rim failure is large and that a probabilistic fatigue life prediction methodology is more appropriate for railroad wheels [31].

It is seen in Fig. 7 that the numerical prediction of the crack shape agrees very well with the field observation. The early stage crack propagation is in a circular configuration, which shows almost equal crack propagation in both minor and major axis directions. Then the crack propagates in an elliptical manner, which is mainly along the major axis direction (track direction). Both numerical prediction and field observations show a compressed contour in the minor axis direction and extruded contour in the major axis direction.

4. Parametric study

In this section, the influence of several factors on the fatigue damage of the wheels is studied, using the developed methodology described above. These factors are wheel diameter, vertical loading, crack length, crack orientation, crack depth and crack face friction coefficient. All other parameters are according to the [32]. The details about the parametric study are shown below.

The diameter of the wheel will affect the fatigue damage. One simple explanation is that the radius of the wheel will affect the internal stress in the wheel according to the Hertz theory. However, for non-linear contact analysis and multiaxial fatigue analysis, the relationship between fatigue life and wheel diameter needs to be studied more carefully. A set of numerical simulations of wheels with different diameters, from 0.711 m (28 in.) to 0.965 m (38 in.) [26], are used. The vertical loading uses the maximum design load for 0.914 m (36 in.) wheel [26]. The equivalent mixed-mode stress intensity factor ranges for different wheel sizes are shown in Fig. 8. From Fig. 8, it is seen that the equivalent mixed-mode stress intensity factor ranges decreases as the wheel diameter increases. It is interesting to notice that the mixed-mode SIF range exhibits a local maximum for the 0.914 m (36 in.) wheel, which indicates larger fatigue damage for this type of wheel. This phenomenon has also been observed by Liu et al. [4] and Ekberg [33] using classical S–N curve-based fatigue analysis.

The equivalent SIFs for the 0.914 m (36 in.) wheel under different vertical loads (58.5 kN, 102.3 kN, 146.2 kN, 175.4 kN and 219.3 kN) are calculated and shown in Fig. 9. The equivalent SIF increases as the vertical load increases almost linearly. For different points at the crack front, the slopes change slightly.

The effects of different crack lengths are shown in Fig. 10. A 0.914 m (36 in.) railroad wheel under 146.2 kN vertical loading with different semi-minor axis length (1 mm, 3 mm, 5 mm, 10 mm and 15 mm) are calculated. Different behaviors are observed for the SIF along the major axis and at the minor axis.

At point 1 on the major axis (see Fig. 1d), the SIF range increases as the crack length increases. The crack length is defined as the semi-minor axis length of the crack. For relatively short cracks, the increase is significant. For long cracks, the increase is small. The reason is that the high stress only occurs within a small region near the contact location. The stress in other parts of the wheel is almost zero at a certain time instant. When the crack is long enough to extend beyond the stressed region, the crack beyond the stressed region has

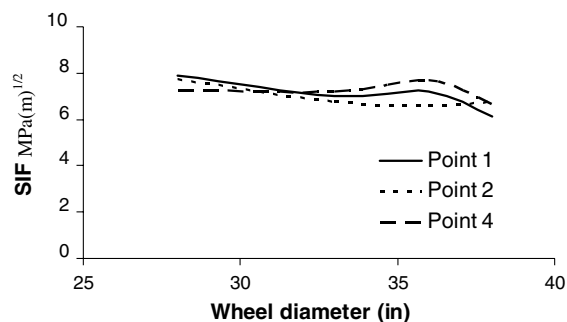


Fig. 8. Wheel diameter effect on SIF range.

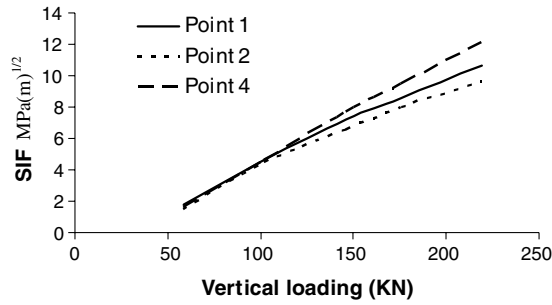


Fig. 9. Loading effect on SIF range.

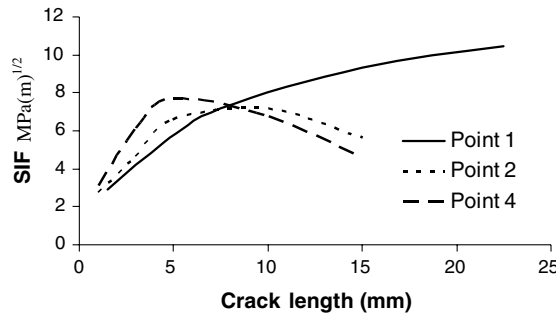


Fig. 10. Crack length effect on SIF range.

little effect on the stress field around the crack tip and the SIF. The long crack experiences almost the same SIF range during one evolution of the wheel.

At points 2 and 4 on the minor axis (see Figs. 1d and 11), the SIF range does not change monotonically as the crack length increases. For short cracks, the SIF increases as the crack length increases. For long cracks, the SIF decreases as the crack length increases. The reason is that long cracks extend beyond the stressed region near the contact location and the crack tip experiences less stress compared with the case when the crack tip is within the stressed region. This is the reason the crack contour is compressed along the minor axis in Fig. 7.

A railroad wheel with diameter 0.914 m (36 in.) under 146.2 kN vertical loading with different crack orientations (0°, 10°, 20° and 30°) is analyzed. The SIFs for different crack orientations are shown in Fig. 11. From Fig. 11, the SIF changes slightly with respect to the crack orientation. For points 1 and 4, the SIF experiences a local maximum between 20° and 30°. This possibly explains why different cracks observed in field show similar orientations, about 20° to the tread surface.

A railroad wheel with diameter 0.914 m (36 in.) under 146.2 kN vertical loading with different crack depths (3 mm, 4 mm, 5 mm, 6 mm, 7 mm and 8 mm below the tread surface) is analyzed. The SIF ranges of different

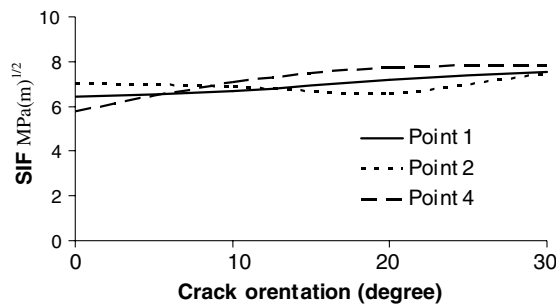


Fig. 11. Crack orientation effect on SIF range.

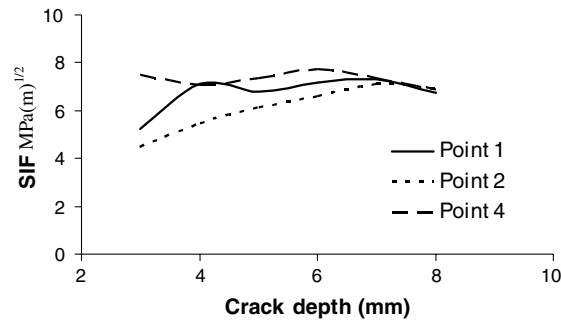


Fig. 12. Crack depth effect on SIF range.

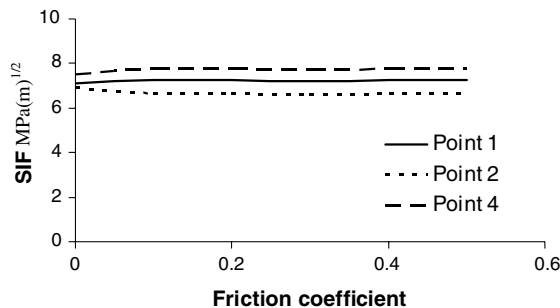


Fig. 13. Crack surface friction coefficient effect on SIF range.

crack depths are shown in Fig. 12. From Fig. 12, the SIF does not change monotonically with respect to different crack depths. The SIF experiences a local maximum around a depth of about 6–7 mm. According to the field observation we collected, subsurface cracks usually initiates at the depth between 5 mm and 10 mm. After initiation, cracks usually propagate parallel to the wheel tread surface at this depth. In the field observations, cracks can deviate to a depth of some 20 mm. However, the growth deviating to the vertical direction is not considered in this study.

A railroad wheel with diameter 0.914 m (36 in.) under 146.2 kN vertical loading with different crack face friction coefficients (0, 0.1, 0.2, 0.3, 0.4 and 0.5) is analyzed. The SIF values for different crack face friction coefficients are shown in Fig. 13. From Fig. 13, the crack face friction coefficient has little effect on the SIF range and its effect can be ignored under the investigated situations. This result is somewhat surprising and we expected the friction effects to be significant before we performed the simulation. However, the simulation results show that the friction effect is not significant under the current conditions. The reasons for this phenomenon can be explained from the following three aspects. (1) Due to the high stress gradient under contact conditions, the normal stress below the surface decreases quickly. This has been discussed in our previous study [4] for railroad wheels. According to the Coulomb friction model employed in this research, the effect of friction is smaller for a subsurface crack compared to a surface crack. (2) The maximum normal stress and shear stress are not proportional to each other under rolling contact loading, which means they do not achieve maxima at the same time instant (see Fig. 8 in [4]). For the current subsurface fatigue crack problem, the delta K depends on the applied maximum shear stress (mode II/III) and the friction stress at the time when the shear stress achieves maxima. The non-proportionality of the normal and shear stress reduces the effect of the friction stress.

5. Conclusion

A general subsurface fatigue crack propagation model under rolling contact conditions of railroad wheels is developed in this paper, which combines a 3D finite element computational method and a previously developed mixed-mode crack propagation model. The non-linear finite element analysis is used for stress intensity

factor computation. A numerical example is implemented and compared with field observations of the failure pattern. The effects of several parameters, namely wheel diameter, vertical loading, crack length, crack orientation, crack depth and crack face friction, on the equivalent stress intensity in railroad wheels are studied using the proposed model.

Several conclusions can be drawn under the investigated conditions in the current study:

- (1) The finite element results show that the stress intensity factor histories of an embedded subsurface crack in railroad wheels under rolling contact conditions are not proportional to each other, which requires that the fatigue analysis must be performed using a fatigue model capable of non-proportional loading.
- (2) For the subsurface crack under rolling contact condition, the mode I stress intensity factor is not significant compared with the mode II and mode III stress intensity factors as the material is under overall compressive loading. Both mode II and mode III components are significant and should be included in the fatigue analysis, which indicates a 2D model is not appropriate for railroad wheels under the current conditions.
- (3) Both field observations and numerical predictions show that the subsurface crack propagates in an “annular ring” pattern. The early stage crack propagation is in a circular configuration, which shows almost equal crack propagation in both axle and track directions. Then the crack propagates in an elliptical manner, which is mainly along the track direction. Both numerical prediction and field observations show a compressed contour in the minor axis direction and extruded contour in the major axis direction.
- (4) Parametric study shows that the vertical loading, crack length, wheel diameter, crack depth and crack orientation have relatively significant effects on the subsurface stress intensity factor ranges. The effect of the friction coefficient between the two crack surfaces is not significant in the current study.

The proposed methodology for rolling contact fatigue analysis offers several advantages compared to most existing models: (1) it employs a 3D elasto-plastic finite element analysis, which represents realistic wheel and rail profiles and gives accurate stress response under rolling contact condition. This is especially useful when the contact conditions cannot satisfy the assumptions of analytical Hertz contact theory; (2) it uses a sub-modeling technique to reduce the computational cost significantly. This characteristic is very useful for future probabilistic analysis to include various uncertainties, which requires many FE analyses to study the effects of random input variables; (3) it uses a mixed-mode crack growth model, which is capable of non-proportional cyclic loadings. As shown in this paper, the subsurface crack is under non-proportional loading conditions and requires such a model for fatigue life prediction.

This paper focused on deterministic mechanic modeling of subsurface crack propagation. For the life prediction of railroad wheels under realistic service conditions, a probabilistic approach considering variabilities in loading spectra, material properties and structural details is required and needs further study. Also, other effects influencing the shattered rim failure, such as manufacturing process parameters, residual stress and brake thermal loading need to be investigated in the future.

Acknowledgements

The research reported in this paper was supported by funds from Union Pacific Railroad and Meridian Railroad (Research Agreement No. 18140, Monitor: Rex Beck). The support is gratefully acknowledged.

References

- [1] Tournay HM, Mulder JM. The transition from the wear to the stress regime. *Wear* 1996;191:107–12.
- [2] Johnson KL. The strength of surfaces in rolling contact. In: *Proc Inst Mech Eng (IMechE)* 1989;203:151–63.
- [3] Ekberg A, Kabo E. Fatigue of railway wheels and rails under rolling contact and thermal loading—an overview. *Wear* 2005;258:1288–300.
- [4] Liu Y, Stratman B, Mahadevan S. Fatigue crack initiation life prediction of railroad wheels. *Int J Fatigue* 2006;28(7):747–56.
- [5] Stone DH, Majumder G, Bowaj VS. Shattered rim wheel defects and the effect of lateral loads and brake heating on their growth. In: *ASME international mechanical engineering congress and exposition*. New Orleans, Louisiana, 1–4 November 2002.

- [6] Giammarise AW, Gilmore RS. Wheel quality: a north American locomotive builder's perspective. GE Research & Development Center, CRD140, September 2001.
- [7] Bernasconi A, Filippini M, Foletti S, Vaudo D. Multiaxial fatigue of a railway wheel steel under non-proportional loading. *Int J Fatigue* 2006;28:663–72.
- [8] Guo YB, Barkey ME. Modeling of rolling contact fatigue for hard machined components with process-induced residual stress. *Int J Fatigue* 2004;26(6):605–13.
- [9] Fatemi A, Socie DF. A critical plane approach to multiaxial fatigue damage including out-of-phase loading. *Fatigue Fract Engng Mater Struct* 1988;11:149–65.
- [10] Šraml M, Flašker J, Potrč I. Numerical procedure for predicting the rolling contact fatigue crack initiation. *Int J Fatigue* 2003;25(7):585–95.
- [11] Ringsberg JW. Life prediction of rolling contact fatigue crack initiation. *Int J Fatigue* 2001;23(7):575–86.
- [12] Jiang Y, Sehitoglu H. A model for rolling contact failure. *Wear* 1999;224:38–49.
- [13] Ekberg A, Bjarnehed H, Lundén R. A fatigue life model for general rolling contact with application to wheel/rail damage. *Fatigue Fract Engng Mater Struct* 1995;18:1189–99.
- [14] Dang Van K. Criterion for high cycle fatigue failure under multiaxial loading. In: *Biaxial and multiaxial fatigue*. London: Mechanical Engineering Publications; 1989. p. 459–78.
- [15] Guagliano M, Vergani L. Experimental and numerical analysis of sub-surface cracks in railway wheels. *Engng Fract Mech* 2005;72:255–69.
- [16] Guagliano M, Vergani L, Vimercati M. Determination of stress intensity factors for three-dimensional subsurface cracks in hypoid gears. *Engng Fract Mech* 2006;73:1947–58.
- [17] Lansler E, Kabo E. Subsurface crack face displacements in railway wheels. *Wear* 2005;258:1038–47.
- [18] Bogdański S, Trajer M. A dimensionless multi-size finite element model of a rolling contact fatigue crack. *Wear* 2005;258:1265–72.
- [19] Glodež S, Ren Z. Modelling of crack growth under cyclic contact loading. *Theor Appl Fract Mech* 1998;30:159–73.
- [20] Cho SS, Komvopoulos K. Finite element analysis of subsurface crack propagation in a half-space due to a moving asperity contact. *Wear* 1997;209:57–68.
- [21] Komvopoulos K. Subsurface crack mechanisms under indentation loading. *Wear* 1996;199:9–23.
- [22] Liu Y, Mahadevan S. Multiaxial high-cycle fatigue criterion and life prediction for metals. *Int J Fatigue* 2005;7(7):790–800.
- [23] Feng M, Ding F, Jiang Y. A study of loading path influence on fatigue crack growth under combined loading. *Int J Fatigue* 2006;28:19–27.
- [24] Liu Y, Mahadevan S. Threshold intensity factor and crack growth rate prediction under mixed-mode loading. *Engng Fract Mech* 2007;74:332–45.
- [25] ANSYS. ANSYS theory reference, release 7.0. ANSYS Inc., 2003.
- [26] AAR (Association of American Railroads). Manual of standards and recommended practices: section G—wheels and axles. M-107/208, issue of 1998.
- [27] Kitagawa H, Takahashi S. Applicability of fracture mechanics to very small cracks or cracks in early stage. In: *Proceedings of the second international conference on mechanical behavior of materials*. Metal Park (OH, USA): ASM International; 1976. p. 627–31.
- [28] Landau LD, Lifschitz EM. *Mechanics*. 3rd ed. Oxford, England: Pergamon Press; 1976.
- [29] Kuna M, Springmann M, Mädler K, Hübner P, Pusch G. Fracture mechanics based design of a railway wheel made of austempered ductile iron. *Engng Fract Mech* 2005;72:241–53.
- [30] Walker EK. The effect of stress ratio during crack propagation and fatigue for 2024-T3 and 7076-T6 aluminum. In: *Effect of environment and complex load history on fatigue life*. ASTM STP, 462. Philadelphia: American Society for Testing and Materials; 1970. p. 1–14.
- [31] Liu Y, Stratman B, Liu L, Mahadevan S. Multiaxial fatigue reliability of railroad wheels. *Reliab Engng Syst Saf*, in press, doi:10.1016/j.res.2006.12.021.
- [32] AAR standard, S-660-83, 1984.
- [33] Ekberg A. Rolling contact fatigue of railway wheels – towards tread life prediction through numerical modelling considering material imperfections, probabilistic loading and operational data. PhD-thesis, Chalmers University of Technology, Department of Solid Mechanics, Göteborg, Sweden, 2000.